PAPER • OPEN ACCESS

A plant-inspired robot with soft differential bending capabilities

To cite this article: A Sadeghi *et al* 2017 *Bioinspir. Biomim.* **12** 015001

View the article online for updates and enhancements.

Related content

- Physical root–soil interactions
  Evelyne Kolb, Valérie Legué and Marie-Béatrice Bogeat-Triboulot

- A novel tracking tool for the analysis of plant-root tip movements
  A Russino, A Ascrizzi, L Popova et al.

- An efficient soil penetration strategy for explorative robots inspired by plant root circumnutation movements
  Emanuela Del Dottore, Alessio Mondini, Ali Sadeghi et al.

Recent citations

- True Low-Power Self-Locking Soft Actuators
  Seung Jae Kim *et al*

- An efficient soil penetration strategy for explorative robots inspired by plant root circumnutation movements
  Emanuela Del Dottore *et al*

- Toward Energy Autonomy in Heterogeneous Modular Plant-Inspired Robots through Artificial Evolution
  Frank Veenstra *et al*

Bioinspiration & Biomimetics

PAPER

A plant-inspired robot with soft differential bending capabilities

A Sadeghi[1], A Mondini[1], E Del Dottore[1,2], V Mattoli[1], L Beccai[1], S Taccola[1], C Lucarotti[1,2], M Totaro[1] and B Mazzolai[1,3]

[1] Center for Micro-BioRobotics, Istituto Italiano di Tecnologia (IIT), Pontedera, Pisa I-56025, Italy
[2] BioRobotics Institute, Scuola Superiore Sant'Anna, Pisa, Pontedera, Pisa I-56025, Italy
[3] Author to whom any correspondence should be addressed.

E-mail: ali.sadeghi@iit.it, alessio.mondini@iit.it and barbara.mazzolai@iit.it
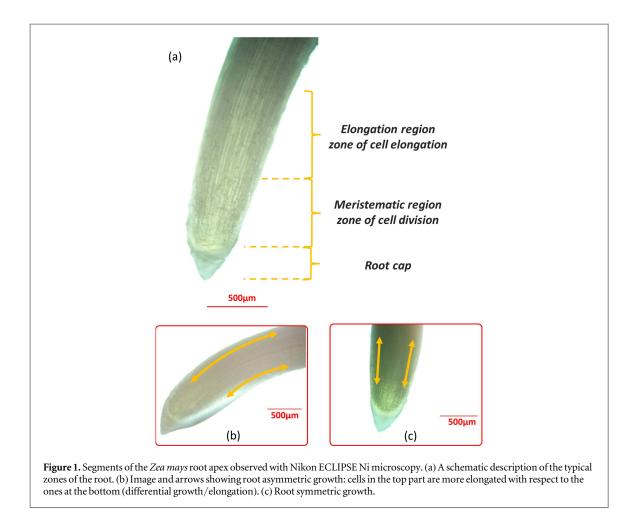
Abstract

We present the design and development of a plant-inspired robot, named Plantoid, with sensorized robotic roots. Natural roots have a multi-sensing capability and show a soft bending behaviour to follow or escape from various environmental parameters (i.e., tropisms). Analogously, we implement soft bending capabilities in our robotic roots by designing and integrating soft spring-based actuation (SSBA) systems using helical springs to transmit the motor power in a compliant manner. Each robotic tip integrates four different sensors, including customised flexible touch and innovative humidity sensors together with commercial gravity and temperature sensors. We show how the embedded sensing capabilities together with a root-inspired control algorithm lead to the implementation of tropic behaviours. Future applications for such plant-inspired technologies include soil monitoring and exploration, useful for agriculture and environmental fields.

1. Introduction

Life and technology greatly depend on resources available in soil. Soil is a source of vital elements (water, nutrients, and minerals) for all living systems, it contains much of the energy resources used by humanity, and it provides precious elements that enable technological advancement. Therefore, soil exploration and monitoring is extremely important for the preservation of life on this planet. Robotics and ICT technologies could help in better identifying potentially interesting or hazardous areas as well as monitoring levels of essential elements or geological properties. Yet, the technology for soil exploration and monitoring is very poorly developed compared to technologies available for exploration and monitoring above the ground. This situation is partly due to the fact that the physical constraints of underground operation strongly challenge an autonomous agent, like a robot.

The development of novel principles for soil penetration, sensory detection, and autonomous decision making could open up new horizons in robotics: autonomous agents able to localise a subsoil source could be used in order to find water and other relevant substances, or to detect the presence of dangerous pollutants to minimise soil contamination. These robotic autonomous systems may find many applications in different scenarios: for environmental monitoring, for efficient and sustainable agriculture, for localising hidden explosives, for automatic humanitarian demining, for rescue tasks after accidents or natural disasters, or for space explorations.

Innovative and performing solutions to achieve this goal can be obtained by studying and investigating the Plant Kingdom. Plants represent the best example among living beings of efficient soil exploration and detection. In particular, roots are the organs delegated to the foraging and the anchoring of plants. While performing these tasks, roots need to adapt to the environment, avoid obstacles, penetrate soil having different mechanical impedances, and follow nutrient and water gradients. The root movement is mediated by sensory feedbacks, being the sensing capabilities mainly located at the root apical part. The responses of the roots to environmental interactions and stimuli are called *tropisms*. They are classified as positive, if there is an attractive response of the root to the stimulus (in this case, the root tends to grow in the stimulus direction), or negative, in the case of a repulsive

Figure 1. Segments of the *Zea mays* root apex observed with Nikon ECLIPSE Ni microscopy. (a) A schematic description of the typical zones of the root. (b) Image and arrows showing root asymmetric growth: cells in the top part are more elongated with respect to the ones at the bottom (differential growth/elongation). (c) Root symmetric growth.

response (i.e., the root grows away from the stimulus) [1, 2]. In order to move towards or far from an environmental stimulus, roots must grow. This phenomenon is mediated by two continuous processes in the apex: cell division and cell elongation. These processes occur in the meristematic and elongation zones, respectively [3]. The main zones of the root are represented in figure 1. The young cells of the root elongate by taking up water and function as a series of miniature linear flexible (soft) 'actuators' that push the root tip into the soil. The symmetric growth of cells at the root sides results in a straight penetration of the root, while asymmetric cell growth (or division) is responsible for a bending and steering behaviour (differential growth/elongation) [3].

Taking inspiration from the biological features of plants and plant roots we have recently developed innovative technologies, including self-growing penetration devices [4], osmotic actuators and mechanisms [5, 6], and soft devices [7, 8]. Indeed, the ability of plants to collect and manage many and different types of inputs at the same time can be an important source of inspiration for control strategies as well, especially for developing new control algorithms for navigation in subsoil environments.

This work aims to develop a plant root-inspired robot, named Plantoid, which merges technical solutions derived from the study of root bending via

differential elongation, sensing capabilities, and associated tropism-behaviours. The preliminary idea of a mechatronic system able to follow environmental stimuli was published in [5]. However, the technological solutions and the level of maturity presented in this manuscript this nwe work deeply different. Specifically, the main novelties presented in this manuscript are listed in the following:

- the actuation system based on three springs which allows the robotic root to orient in each direction instead of having a limited set of positions;

- a new humidity sensor for soil moisture based on PEDOT:PSS/iron oxide NPs nanofilms l;

- a deeper integration of sensors for tropisms (two additional sensors for touch and temperature detection were added and integrated in the tip);

- a new control algorithm.

Current work presents the design and fabrication of sensorized tips, with commercial and customised sensors suitable for soil monitoring, and the robot behaviour inspired by plant root tropisms. In order to better observe and validate the robot behaviour and the sensing capabilities, we tested them in air by means of a robotic platform integrating soft actuators for root

differential bending. The latter can be included in a category of soft linear actuator solutions conceived to steer soft robotic arms [9].

Most actuation approaches are based on pneumatic/fluidic systems or wire-based systems. Specific examples are OctArm, driven by braided fluidic actuators [10, 11]; flexible micro actuator (FMA), developed using elastic chambers radially reinforced by fibres [12]; tendon-driven mechanisms [13–15]; and shape memory alloy (SMA) driven mechanisms [16, 17]. In arms made using wire-based actuators, the bending occurs by differential pulling of wires (tendon-based) or retraction of actuators (SMA), but in the case of fluidic based actuators, bending can be obtained by differential elongation/retraction, depending on the orientation of flow (positive/negative pressure) or on the type of actuators. SMA-based actuators can have good characteristics in terms of integrability, but they require high power. Also, the high temperature generated by SMA operation would cause the accumulation of temperature that in the cases which require temperature sensing (e.g. the artificial root) affects the proper functioning of temperature sensors. Most of the soft fluidic actuators can perform efficient work mainly in one direction: in retraction, like braided fluidic actuators [18], or in elongation, like radially reinforced elastic chambers [12]. Combination of fluidic and wire-based actuation principles can lead to an antagonistic actuation mechanism [19–21]. In our case we required the artificial root to make a differential bending without using bulky components (e.g., pipes, valves, and pumps), imposing a challenging integration process for the development of small-scale systems. Hence, although the fluidic-based mechanism is attracting for our application, in this work we present a soft bending mechanism with differential elongation capabilities based on DC motors and helical springs. The presented actuator can perform both retraction and elongation actions these properties permit development of a root like mechanism that mainly requires a pushing action which is not intrinsically and easily achievable with cable-driven actuation. Moreover, we describe our robotic platform with the three soft bending roots that we use to test a stimulus-oriented control, which imitates the plant root behaviour, and we demonstrate the ability of an individual robotic root to perform tropic responses bending under appropriate stimulation in air.

Respect to more standard pan-tilt mechanisms (i.e. with two motors, each with series elastic outputs to add compliance), the reported approach has two main key advantages: first, it is more easy to implement and miniaturise (no joint assembly is necessary), also given the less stringent requirements in terms of accuracy and assembly process; second, the behaviour and control of the spring-based mechanism imitate the real plant since the spring elongation can be strictly related to the cell elongation, simplifying the bioinspired stimulus-driven control.
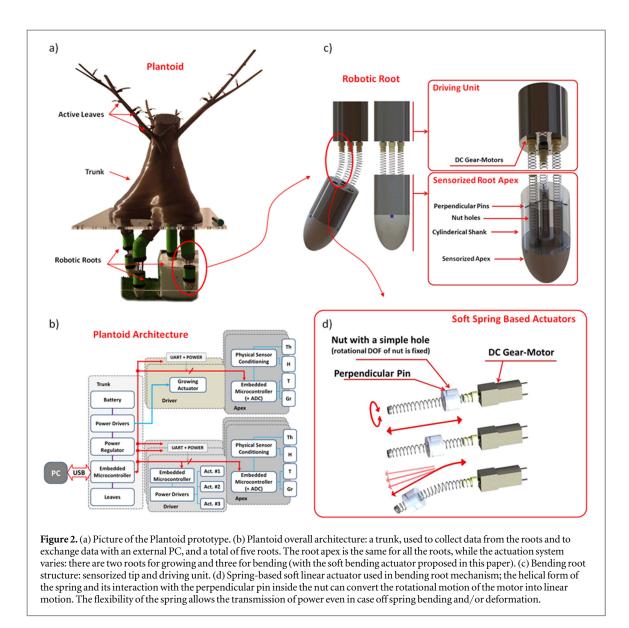
2. The plant-inspired robot

2.1. The plantoid architecture

The proposed plant-inspired robot (Plantoid) (see figure 2(a)) consists of a trunk, a number of functional roots with sensorized apexes, and an aerial part with leaves (based on a controllable hygromorphic plant-inspired material [7]). All the roots are connected to a trunk that acts as a gateway to transfer data and configuration parameters to the external world (through a USB connection with a graphical user interface developed in MATLAB). In nature, each root apex can be considered as a command centre [22] that interacts with its neighbours without a central decision unit, causing emergent behaviour [23]. Analogously, Plantoid has no central decision unit, but each artificial root has its own controller to implement the behaviour. Each root consists of two subsystems: a sensorized root apex and a root driving unit. The root apex is dedicated to data acquisition from the sensors and to the implementation of the high-level algorithm that, based on the acquired data, defines the growth direction. The root driving unit implements a low-level control by driving the growing or bending actuators, depending on the type of root connected. In this implementation, there are three bending roots (described in detail below) and two growing roots (described in detail elsewhere [4]). Hence, the driving unit can be easily changed (without changing the apical part) according to the specific actuation system. The general architecture of Plantoid is reported in figure 2(b). The two subsystems (figure 2(c)) are connected by three sets of our soft spring-based actuators (SSBA). The details of the actuation system and bending architecture are described below.

2.2. Design of the SSBA and the bending root

Among conventional mechanical components, springs can provide flexibility and compliance to rigid structures based on the stiffness of their materials and their particular shapes. In this work, we benefit from both the flexibility and shape of helical springs to transmit the motor power in a compliant manner. Similarly to the nut-screw mechanism, which is traditionally used to convert the motor rotation in a linear motion, we used a helical spring (instead of a screw) to obtain a linear actuation. The result is a soft linear actuator that can transmit the rotary motor power to a linear motion even after bending or buckling in the spring (figure 2(d)). Each SSBA includes a DC gear-motor (Pololu Micro Metal Gearmotor with gear ratio of 986:41, maximum speed of 32 RPM and maximum torque of 9 kg cm^{-1}) connected to a steel helical spring (helix pitch 2.4 mm, external diameter 6 mm, wire diameter 0.5 mm, and elastic constant K 2.13 $\times$ 10^3 N m^{-1} in case of 30 mm spring length) attached on one side to the shaft of the motor and on the other side passes through the hole of

Figure 2. (a) Picture of the Plantoid prototype. (b) Plantoid overall architecture: a trunk, used to collect data from the roots and to exchange data with an external PC, and a total of five roots. The root apex is the same for all the roots, while the actuation system varies: there are two roots for growing and three for bending (with the soft bending actuator proposed in this paper). (c) Bending root structure: sensorized tip and driving unit. (d) Spring-based soft linear actuator used in bending root mechanism; the helical form of the spring and its interaction with the perpendicular pin inside the nut can convert the rotational motion of the motor into linear motion. The flexibility of the spring allows the transmission of power even in case off spring bending and/or deformation.

a particular nut (figure 2(d)). The DC gear motor can directly rotate the spring by fixing the rotational DOF of the nut; the rotation of the spring can impart a linear motion to the nut. The nut is actually a simple hole in a solid material with a metal pin perpendicular to the axis of the hole (figure 2(d)). The spring passes through this hole and interacts with the metal pin to push or pull the nut along its axis (figure 2(c)).

Each bending root includes three SSBAs, located at 120° each other and distant 13 mm from the body centre (figure 2(c)). The holes of all three nuts of SSBAs are axially embedded in the cylindrical shank of the sensorized root apex. The final assembly can interact safely with the environment, due to the flexibility of the springs, which act as the interface between the driving unit and the sensorized apex. Moreover, the sensorized apex can actively move in a 3D space by means of the three SSBAs. Each SSBA can operate in both elongation and retraction directions, simply by changing the rotation wise in the DC motor. The robotic root can elongate in a straight direction when all three SSBAs elongate at the same speed, and can

perform bending and steering behaviours when the elongation velocity of SSBAs is different (differential elongation). Each complete rotation of the DC gear-motor shaft results in a complete rotation of the spring, causing an elongation equal to the pitch (P) of the helix in the spring. Assuming that the pitch of the spring remains constant for the β degree rotation of the DC gear motor shaft, then the Δl elongation of each SSBA and the whole length of the actuator l (the portion of the spring free to bend) can be obtained by

$$l = l_n + \Delta l = l_n + \frac{\beta}{360}P, \tag{1}$$

where l_n is the initial length of the free portion of the spring.

Therefore, the elongation speed (S_L) is simply a function of the rotation speed of the DC gear-motors and the pitch of the helical springs:

$$S_L = \frac{M_S}{60}P = \frac{N}{60}\left(P_0 - \frac{F_W}{NK}\right), \tag{2}$$

where M_S is the DC motor speed in rpm, F_W is the applied force, P_0 is the initial pitch of the spring

Table 1. Maximal axial forces of a single SSBA, acquired with the INSTRON 4464, at different initial spring length, and its standard deviation. The experiments have been performed in two conditions: pushing on the load cell by elongating the spring, and pulling the load cell by contracting the spring (inverting the motor rotation).

Initial length (mm)	12		24		36	
	Max. force (*N*)	Std. Dev.	Max. force (*N*)	Std. Dev.	Max. force (*N*)	Std. Dev.
Spring elongation	16.86	0.60	7.83	0.46	5.15	0.67
Spring contraction	17.47	1.48	17.09	0.80	14.07	0.69

without load, K is the spring constant and N is the number of active coils.

The proposed actuator is a sort of bendable lead screw. Such kinds of devices are described in terms of lifting axial force and torque. In particular, the force can be expressed as:

$$F_w = \frac{T}{r\frac{\sin\alpha + \mu\cos\alpha}{\cos\alpha - \mu\sin\alpha}}, \tag{3}$$

where T is the torque, r is the spring radius, μ is the friction coefficient and where α is defined as:

$$\alpha = \tan^{-1}\frac{P}{2\pi r}. \tag{4}$$

In the spring case, pitch is not constant, since under compression the pitch decreases. This variation directly affects the force that the actuator can contrast. Indeed, it increases when the spring pushes/grows (lower pitch), while the opposite effect occurs in the pulling case. However, the equation (3) is acceptable without spring buckling. Buckling happens more easily with longer spring. Indeed, approximating it to an elastic column, the maximum axial load before buckling is proportional to $1/l^2$, with l the spring length [24]. The forces reachable by a single SSBA range from a minimum of about 5 N up to 17 N depending on the spring starting length (12, 24, 36 mm) and rotation direction, as shown in table 1, reaching an S_L of 1.28 mm s^{-1}.

The final curvature angles and the arc length of the bending mechanism based on SSBAs can be calculated considering the final length of each spring as defined in the Webster and Jones's equation [25].

The mechanism can be described in terms of arc parameters, namely curvature (κ), plane (Φ), and arc length (l):

$$l = \frac{l_1 + l_2 + l_3}{3}, \tag{5}$$

$$\phi = \tan^{-1}\left(\frac{\sqrt{3}(l_2 + l_3 - 2l_1)}{3(l_2 - l_3)}\right), \tag{6}$$

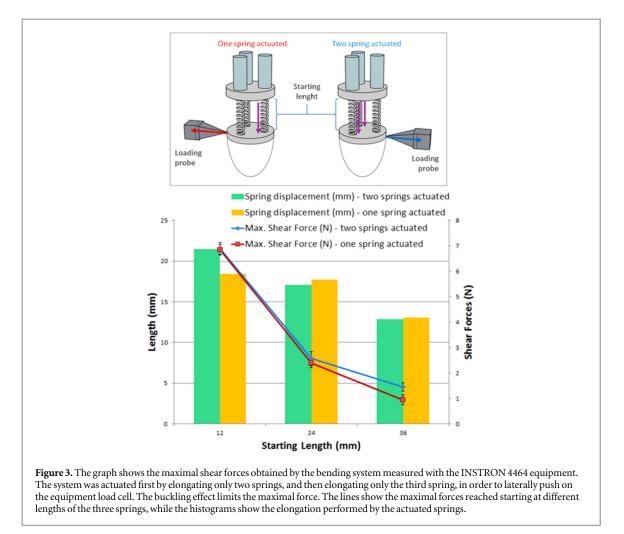$$\kappa = \frac{\sqrt{l_1^2 + l_2^2 + l_3^2 - l_1 l_2 - l_1 l_3 - l_2 l_3}}{d(l_1 + l_2 + l_3)}, \tag{7}$$

where l_i are the length of the actuators (defined in (1)) and d is the distance of each actuator from the body centre.

One of the main hypotheses of this model is that neither compression nor elongation occurs in each spring. This is nearly true in air, where only the weight of the tip causes a small deviation between the theoretical position and the real position, but it is not true in soil, even in a relative loose medium. Then, in this case a compensation for the spring deformation is necessary, which can be performed by measuring the force acting on the spring and increasing or decreasing its length consequently.

This kind of model, which permits to control the bending mechanism in a 3D space, can be useful for manipulation tasks, where force control, precision in reaching a target, and a specific path planning control are important. Instead, in order to control a robotic root in an unknown environment, for instance in soil for exploration and monitoring purposes, the implementation of a plant root inspired behaviour seems more suitable. Indeed, for these kinds of applications we do not have an absolute position to reach, neither a specific pre-determined path to follow, and the classical kinematic approach becomes not convenient. SSBAs are here instead controlled with a stimulus-oriented approach and the robotic root is able to follow the environmental stimuli. Then, the important parameters to model are the direction along the axis parallel to the ground and the inclination with respect to the vertical axis. Such a kind of control can be obtained by actuating the springs till the accelerometer, placed in the apex, reaches the correct position (as explained in detail in section 2.6), and the compensation of compression/elongation of the springs are in this case automatically applied by the control without caring about the spring lengths. Also, we should note that, following this approach, we can reach the same final configuration with different sets of rotation sequences applied to the three DC motors.

In our system we selected the minimum spring length that allows a reasonable bending for testing the tropic behaviour, which is 15 mm. In particular, with this value we obtained a maximum bending angle of 59° at 7.5° s^{-1}. In such conditions we compared the root apex orientation (measured with an embedded accelerometer) with that predicted by equations (5–7), obtaining a maximum deviation of ~4°.

We measured the lateral forces of the bending using a universal testing machine (INSTRON 4464). The maximal force is defined as the lateral force that the spring is able to provide before buckling (see figure 3). Similarly to the case of a single actuator, the maximal force achievable by the system depends on

Figure 3. The graph shows the maximal shear forces obtained by the bending system measured with the INSTRON 4464 equipment. The system was actuated first by elongating only two springs, and then elongating only the third spring, in order to laterally push on the equipment load cell. The buckling effect limits the maximal force. The lines show the maximal forces reached starting at different lengths of the three springs, while the histograms show the elongation performed by the actuated springs.

the initial length imposed to the springs and, as already anticipated, the buckling effect occurs earlier with longer initial length. This behaviour is visible in the histograms reported in figure 3, which show shorter elongation achieved by the longer springs before reaching the maximal force. The critical total length of the spring registered by our system is in the range of approximately 30–50 mm, by imposing a load up to 7 N, limits far from our range of movements and loads. The results obtained by actuating one or two springs are similar, as shown in figure 3. Indeed, since the centre of rotation is at the centre of the tip, then in the case of double spring the lever arm is half of the single spring case. Hence, considering the force generated by each spring as fixed, the product yielding the torque (lever arm *x* force) is the same.

2.3. Design of the sensorized root apex

The sensorized root apex is devoted to the perception of the environment and the control of the root behaviour. The apex integrates four types of sensors that are fundamental to validate the robot behaviour inspired by plant root tropisms responding to the following environmental stimuli: gravity (detected using a commercial three-axis accelerometer, LIS331DLH from ST Microelectronics), temperature (detected using three commercial temperature

sensors, TMP123 from Texas Instruments), touch (detected using four specifically *ad hoc* developed tactile sensors [26, 27] described in section 2.5) and humidity (detected using three customised soil moisture sensors presented in section 2.4). Sensors are integrated in a root with a maximum diameter of 50 mm. The details of the apex structure, geometry, and sensor integration are shown in figure 4(a).

A built-in microcontroller system (based on a PIC32MX340F512H from Microchip, Inc.) is devoted to the sensor conditioning, data acquisition, to the control algorithm and data communication (see figure 4(b)). Specifically, the temperature and gravity sensors are interfaced through a serial peripheral interface (SPI) bus, with a vendor-specific protocol; the humidity sensors, which are resistive sensors, are measured by a suitable shunt resistor at fixed voltage excitation, using the microcontroller internal ADC; for the conditioning of the tactile sensors, which are capacitive transducers, we used 24 bits capacitance-to-digital converters (AD7147 from Analog Devices) interfaced with the microcontroller unit by SPI bus and vendor-specific protocol. All the acquired data are elaborated by the microcontroller (high level algorithm), and the resulting root bending direction is sent to the root driving unit by a universal asynchronous
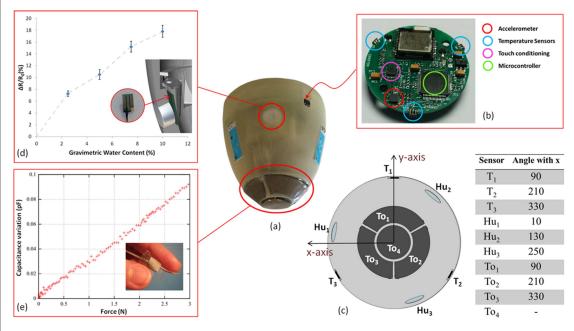
Figure 4. (a) Overview of the robotic root apex. (b) Picture of the electronic board integrated into the apex. (c) Sensor position in the root apex. The x- and y-axes are the axes of the integrated accelerometer, used as a reference. T_n are the temperature sensors, Hu_n are the soil moisture sensors, and To_m are the tactile sensing elements of the array (with $n = 1, 2, 3$ and $m = 1, 2, 3, 4$). The table on the right shows the angle positions of the sensors with respect to the x-axis. Sensors of different type are rotated with respect to one another to avoid mechanical interference. Free space is dedicated to the integration of further sensors. (d) Change in the resistance of PEDOT:PSS nanofilms transferred on flexible Kapton© substrate versus gravimetric water content; in the inset, the sensor is inserted in the apex internal chamber with an embedded filter cap to protect the sensor inside. (e) Characteristics in terms of capacitance variation versus the force of the single tactile sensor obtained through indentation tests at a suitable probing station; in the inset is a sample of the tactile sensor.

receiver–transmitter (UART) interface and custom protocol.

To measure a spatial gradient in soil (in the plane perpendicular to the apex), three sensors for the same stimulus (i.e., humidity and temperature) are placed around the tip at 120° with respect to each other. The tactile sensors are instead integrated at the apex extremity into an array of four sensors to detect and define the position of possible obstacles in the environment. Figure 4(c) shows an overview of the sensor positioning at the apex level.

2.4. PEDOT:PSS humidity sensors

In developing the technological approach for humidity sensing we considered detection of the moisture in a soil medium. Soil moisture sensors are usually large because they are constructed for agriculture applications. In [5], we proposed a soil moisture sensor based on metal electrodes for measuring the impedance of the soil (correlated with the water content).

Although these sensors are very robust and adapted to work in soil, they require good contact between the electrodes and the medium to obtain a reliable measurement, a condition that is difficult to satisfy when the sensor dimensions are scaled down. To overcome this problem, here we propose a new solution based on an ultra-thin film conductive polymer sensor technology. Among other conducting polymers, PEDOT:PSS (poly(3,4-ethylenedioxythiophene) polystyrene sulphonate) has been reported as a water-

absorbing material [28]. This property provides a basis for humidity-sensing applications. In particular, it is known that the resistivity of PEDOT:PSS films increases as RH increases, as observed in [29, 30, 31]. Recently, large-area free-standing conductive ultra-thin films of PEDOT:PSS have successfully been fabricated by our group [32, 33]. Moreover, composite PEDOT:PSS free-standing thin films with embedded iron oxide nanoparticles (NPs) retaining both magnetic and electrical conductivity functionalities were also presented [34]. These free-standing nanofilms can be easily transferred onto various rigid and soft substrates with arbitrary shapes and topographies due to their high conformability, preserving their functionalities. Based on these results, we developed a new sensor for gravimetric water content in soil. The sensor consists of PEDOT:PSS nanofilms over small copper electrodes (1 mm width size, 0.2 mm distance) deposited on a flexible Kapton© substrate (see figure 4(d)). To protect the PEDOT:PSS nanofilms from direct contact with the soil, we packaged them into the root using a tip filter cap (Filter Cap SF1 from Sensirion AG). In details, as shown in the inset of figure 4(d), we inserted the sensor substrate in a small chamber within the root apex, which was then sealed. From the other side, we placed the filter cap. The packaging provides physical protection from scratching and abrasion and avoids the exposure of the sensors to any environmental parameters other than humidity. In fact, with this configuration, the PEDOT:PSS sensors can measure the

air saturation present within the interstitial pore spaces in the soil. Using this approach, soil grain size and texture do not influence the sensor operation. As an example, figure 4(d) reports the change in resistance ($\Delta R/R_0$ (%)) with respect to gravimetric soil water content. Full details on the sensor fabrication, characterisation, and soil measurement are provided in supplementary materials.

2.5. Tactile sensors integration

We integrated a soft tactile sensing array in the root apex following the configuration depicted in figure 4(a). The design is such that tactile information can be retrieved both from the extremity of the apex tip, which is the first region of the robotic root that encounters new soil during exploration, and from the nearby regions [27]. Thus, spatial information about the touch stimulus is provided from the maximum volume of the apex. In detail, three lateral sensing elements (i.e., To_1–To_3, with an area of 115 mm^2) wrap the sides of the apex at 120° to each other, while one sensing element (i.e., To_4, circular, with an area of 78.5 mm^2) is located at the end of the apex. The transduction principle is capacitance-based, and each sensor is built from a combination of different conductive and elastomeric layers. In particular, each sensing element consists of two parallel electrodes, made of soft and flexible copper/tin-coated woven fabric (70 μm thick, Zelt Mindsets Ltd, UK), separated by a silicone elastomeric dielectric layer (Ecoflex® 00-10, Smooth On) [27]. The use of conductive textile for the electrodes appears to be a good choice because, in addition to its electrical and mechanical properties, it can be easily patterned with the desired shape by laser cutting technique (VLS 3.50; universal Laser Systems, Inc., USA). At the same time, the elastomeric dielectric layer can be cast from a solution by spin coating to obtain the target thickness of 300 μm. It is worth emphasising that the sensing system consists of the array together with the read-out electronics, which must be designed and built to resolve the subtle changes in capacitance experienced by the soft sensing elements when they are mechanically stimulated. To this end, the custom electronics are integrated in the board, as described in section 2.3. A typical response in terms of capacitance variation versus force is shown in figure 4(e). In a preliminary study [27], we evaluated the performance of the soft tactile sensing array integrated in the robotic root apex by conducting experiments in which the root apex was able to approach a semispherical obstacle and perform bending movements (according to the tactile feedback provided). In particular, we performed different experimental sessions by modifying the number of sensing elements involved in the root/obstacle contact and by using obstacles made of materials with different mechanical properties.

2.6. The control algorithm

We used the three SSBA roots as platforms to test a stimulus-oriented control which imitates the plant root behaviour, and we demonstrated the ability of the implemented robotic root to perform tropic responses and bend under appropriate stimulation. As previously reported, the plant root apex plays a key role in tropic responses. Analogously, the robotic root has a sensorized apex with a control algorithm that takes as input the sensor data acquisitions and gives as output the direction of bending. Moreover, as in the biological counterpart, in the case of a positive tropism, the algorithm returns the direction towards the stimulus, whereas with a negative tropism, the algorithm returns the direction opposite the stimulus.

The intensity of the stimulus responses varies among different plant species and also among samples of the same species; in addition, the optimal growth conditions in terms of growing temperature, nutrition needs, and water requirements differ among species. This diversity is defined by the DNA of each plant.

Each robotic root is then configured with its starting 'DNA', which encodes information about the optimal environmental conditions as target values to reach. The interplay among tropisms is implemented in the current algorithm through priorities associated to each stimulus, which are expressed in DNA.

The bending direction is obtained by evaluating each single tropism based on the stimulus acquired from each sensor along the apex and combining each tropism result with the appropriate weight given by the priority.

This procedure results in the following equation:

$$R_{(t)} = S_{T(t)} + S_{Hu(t)} + S_{To(t)} + S_{G(t)}, \qquad (8)$$

where $R_{(t)}$ is a three-dimensional vector resulting from the stimulus at time t. The components of the vector are the module or intensity, r, and the angles θ and φ which express the bending direction with respect to a coordinate system integral to the tip (see figure 4(c)). Summing $R_{(t)}$ with the current position in space of the apex, we obtain the next position to reach in the environment. Vector $S_{i(t)}$ (where i here and in the following equations are T, temperature; Hu, humidity; To, touch; and G, gravity) is the single stimulus vector at time t, expressed in the same coordinate system. $S_{i(t)}$ is obtained as follows:

$$S_{i(t)} = f(\text{DNA}, R_{i(t)}). \qquad (9)$$

DNA is the configured DNA of the root, and vector $R_{i(t)}$ is the result of the sensor measurement of the ith stimulus. For each tropism, we obtain the individual contribution $R_{i(t)}$ in terms of module and angle in the reference coordinate system (see also figure S3 in supplementary materials).

2.6.1. Gravity

$$\theta_G = \mathrm{arc}tg\left(\frac{G_y}{G_x}\right), \qquad (10)$$

$$\varphi_G = \text{arc}tg\left(\frac{\sqrt{G_x^2 + G_y^2}}{G_z}\right), \tag{11}$$

G_x, G_y, G_z are the measurements supplied by the accelerometer; θ_G is the angle with respect to the *x-axis* of the projection of the gravity vector on the *x–y* plane; and φ_G is the angle between the tip direction and the gravity vector. The intensity of the stimulus, r_G, is

$$r_G = \sin(\varphi_G). \tag{12}$$

2.6.2. Temperature

$$T_x = |T_1 - T_K| \cdot \cos(\alpha_{T1}) + |T_2 - T_K| \cdot \cos(\alpha_{T2}) \\ + |T_3 - T_K| \cdot \cos(\alpha_{T3}), \tag{13}$$

$$T_y = |T_1 - T_K| \cdot \sin(\alpha_{T1}) + |T_2 - T_K| \cdot \sin(\alpha_{T2}) \\ + |T_3 - T_K| \cdot \sin(\alpha_{T3}), \tag{14}$$

$$r_T = \sqrt{T_x^2 + T_y^2}, \tag{15}$$

$$\theta_T = \text{arc}tg\left(\frac{T_y}{T_x}\right), \tag{16}$$

T_1, T_2, T_3 are the measurements supplied by the three temperature sensors; α_{T1}, α_{T2}, α_{T3} are the angles at which the respective temperature sensors are placed with respect to the *x*-axis in the *x–y* plane; T_K is an ideal temperature, and the 'distance' of each sensor with respect to this temperature is measured. The temperature measurement vector is finally given by r_T, the module of the vector, and θ_T, the angle of the vector with respect to the *x-axis* in the *x–y* plane. As the temperature measurement vector is always in the *x–y* plane, φ_T is always null (analogously to the humidity and touch measurements).

2.6.3. Humidity

$$\text{Hu}_x = \text{Hu}_1 \cdot \cos(\alpha_{\text{Hu}1}) + \text{Hu}_2 \cdot \cos(\alpha_{\text{Hu}2}) \\ + \text{Hu}_3 \cdot \cos(\alpha_{\text{Hu}3}), \tag{17}$$

$$\text{Hu}_y = \text{Hu}_1 \cdot \sin(\alpha_{\text{Hu}1}) + \text{Hu}_2 \cdot \sin(\alpha_{\text{Hu}2}) \\ + \text{Hu}_3 \cdot \sin(\alpha_{\text{Hu}3}), \tag{18}$$

$$r_{\text{Hu}} = \sqrt{\text{Hu}_x^2 + \text{Hu}_y^2}, \tag{19}$$

$$\theta_{\text{Hu}} = \text{arc}tg\left(\frac{\text{Hu}_y}{\text{Hu}_x}\right). \tag{20}$$

Hu_1, Hu_2, Hu_3 are the measurements supplied by the three humidity sensors; α_{Hu_1}, α_{Hu_2}, α_{Hu_3} are the angles at which the respective humidity sensors are placed with respect to the *x*-axes in the *x–y* plane. The humidity measurement vector is finally given by r_{Hu}, the module of the vector, and θ_{Hu}, the angle of the vector with respect to the *x-axis* in the *x–y* plane.

2.6.4. Touch

$$\text{To}_x = \text{To}_1 \cdot \cos(\alpha_{\text{To}1}) + \text{To}_2 \cdot \cos(\alpha_{\text{To}2}) \\ + \text{To}_3 \cdot \cos(\alpha_{\text{To}3}), \tag{21}$$

$$\text{To}_y = \text{To}_1 \cdot \sin(\alpha_{\text{To}1}) + \text{To}_2 \cdot \sin(\alpha_{\text{To}2}) \\ + \text{To}_3 \cdot \sin(\alpha_{\text{To}3}), \tag{22}$$

$$r_{\text{To}} = \sqrt{\text{To}_x^2 + \text{To}_y^2}, \tag{23}$$

$$\theta_{\text{To}} = \text{arc}tg\left(\frac{\text{To}_y}{\text{To}_x}\right). \tag{24}$$

To_1, To_2, To_3 are the measurements supplied by the three lateral sensing elements of the tactile array; $\alpha_{\text{To}1}$, $\alpha_{\text{To}2}$, $\alpha_{\text{To}3}$ are the angles at which the respective sensing elements are placed with respect to the *x*-axis in the *x–y* plane. The touch measurement vector is given by r_{To}, the module of the vector, and θ_{To}, the angle of the vector with respect to the *x-axis* in the x-y plane.

After obtaining the sensor measurement vectors, the value of each stimulus r_i is normalised between 0 and 1 to obtain the new normalised module M_i as in the following equation:

$$M_i = \begin{cases} 0, & \text{if} \quad r_i \leqslant r_i^{\text{Th\_Low}}, \\ \dfrac{r_i - r_i^{\text{Th\_Low}}}{r_i^{\text{Th\_High}} - r_i^{\text{Th\_Low}}}, & \text{if} \quad r_i^{\text{Th\_Low}} \leqslant r_i \leqslant r_i^{\text{Th\_High}}, \\ 1, & \text{else}. \end{cases} \tag{25}$$

where $r_i^{\text{Th\_Low}}$ and $r_i^{\text{Th\_High}}$ are respectively, the lower and higher bound of the valid range for each stimulus, expressed by DNA. Below the minimum value, the stimulus is considered to be absent; above the maximum value, the stimulus is saturated, while in the middle, the resultant value is considered to be linear. The single stimulus vector S_i is then the vector with module M_i and directions defined by θ_i and φ_i in the considered reference coordinate system. Finally, the resulting combined stimuli vector $R_{(t)}$ is calculated as the vector sum of the single stimulus as defined in equation (5).

The proposed root control algorithm, inspired by real plant root behaviours (tropisms), is based on a stimulus-following approach. When a parameter gradient is measured, the algorithm replies to the resulting stimulus by bending in that (or the opposite) direction. This response can also occur against gravity, but because of the importance of gravity, when the two forces compensate each other (become equal), the bending is stopped. With this approach, the vector resulting from all the stimuli (including gravity), which gives the direction θ and the intensity of the differential growth r, are directly used to calculate the motors speeds Sp_j (where subscript j can be 1, 2 or 3) by applying the following formula:

$$Sp_1 = K_G \cdot r_G \cdot \cos(\theta_G) + K_{Hu} \cdot M_{Hu} \cdot \cos(\theta_{Hu}) - K_T \cdot M_T \cdot \cos(\theta_T) - K_{To} \cdot M_{To} \cdot \cos(\theta_{To}), \tag{26}$$

$$Sp_2 = K_G r_G \cos\left(\theta_G - \frac{2\pi}{3}\right) - K_T M_T \cos \\ \times \left(\theta_T - \frac{2}{3}\pi\right) + K_{Hu} M_{Hu} \cos\left(\theta_{Hu} - \frac{2\pi}{3}\right) \\ - K_{To} M_{To} \cos\left(\theta_{To} - \frac{2}{3}\pi\right), \tag{27}$$

$$Sp_3 = K_G r_G \cos\left(\theta_G + \frac{2\pi}{3}\right) - K_T M_T \cos \\ \times \left(\theta_T + \frac{2}{3}\pi\right) + K_{Hu} M_{Hu} \cos\left(\theta_{Hu} + \frac{2\pi}{3}\right) \\ - K_{To} M_{To} \cos\left(\theta_{To} + \frac{2}{3}\pi\right), \tag{28}$$

where K_i are the fixed priorities (configurable between 0 and 1 and s.t. $\sum K_i = 1$) present in DNA, and because M_i are normalised between 0 and 1, Sp_j will also result in a value between 0 and 1 and can be used as power percentages to drive the motors. Sp_j can also be negative due to the reversibility of the linear actuation mechanisms.

The speed of the actuator is indeed dependent on the priorities assigned to the stimulus and on the motor power. By varying priorities and/or motors we can achieve different performance.

3. Experimental trials and results

To evaluate the bending capabilities of the soft actuated artificial roots and the ability of the algorithm to drive the actuation by emulating root behaviour, we performed four set of experiments: one for each integrated tropism. Each experiment had three different priority values for a tropism. The protocol used to evaluate the tropic responses from the artificial root consists of the following steps:

(1) Configure the root with the appropriate DNA;

(2) Fix a starting position for the root;

(3) Run the algorithm and begin recording the sensor output;

(4) Apply a stimulus to the root;

(5) Stop the run after the apex reaches a stable position.

All experiments were performed with the root in air (see also supplementary materials-video 1).

To evaluate the gravitropic response, the apex of the root was initially oriented against gravity. This starting position of the root was also used as the stimulus for gravitropism. In DNA, only K_G was imposed as different from 0, while all the others were equal to 0.

The starting position for hydrotropism, thermotropism, and thigmotropism was fixed towards the gravity vector; due to the essential role of gravity in root behaviour (as previously reported), the priority of gravity was never nullified in the experiments and played an important role in the control algorithm. If the gravity priority level changed, then the point of balance between the stimuli changed and therefore also the bending response changed.

To compare the results, we fixed the values of the priorities at three different representative ratios (arbitrarily chosen) with values in between 0 and 1, as follows:

(1) $K_G = 0.5, K_i = 0.5$, with $i \neq G$,

(2) $K_G = 0.3, K_i = 0.7$, with $i \neq G$,

(3) $K_G = 0.7, K_i = 0.3$, with $i \neq G$.

We made this choice to observe the differences in reaching the point of balance giving equal, more or less priority to one tropism with respect to gravity.

To evaluate the hydrotropic response, the root was stimulated with wetted soil in contact with one of the three sensors integrated in the apex. For the thermotropic response, we imposed the optimal growth temperature value in DNA at 25 °C and used a source of high temperature, specifically a soldering iron, in proximity to the temperature sensor to modify the environmental conditions. Finally, to evaluate the thigmotropic response, we stimulated the root with an obstacle placed under the apex extremity in contact with one of the lateral sensing elements of the tactile array. For each experiment, we acquired 100 samplings of the sensors, within an average of 35 s (sufficient for the system to reach equilibrium in each condition) and recorded the sensor output to post-process the bending response in correlation with the sensor acquisition.

We examined the sensor acquisitions after the experimental trials; the bending of the root in each experiment is here presented in a polar graph, where the radius represents the angle of the tip with respect to the gravity vector (φ_G obtained in (8)) and the polar angle is the direction of bending (θ_G obtained from (7)). Both the radius and the angle are expressed in degrees. Hence, each point represents the relative position of the apex; points closer to the external circumference represent a tip position far from the gravity vector, while points closer to the centre represent a tip position close to the gravity vector. The movement over time is expressed by a grey colour scale: darker points represent initial positions, while lighter points represent final positions of the apex.
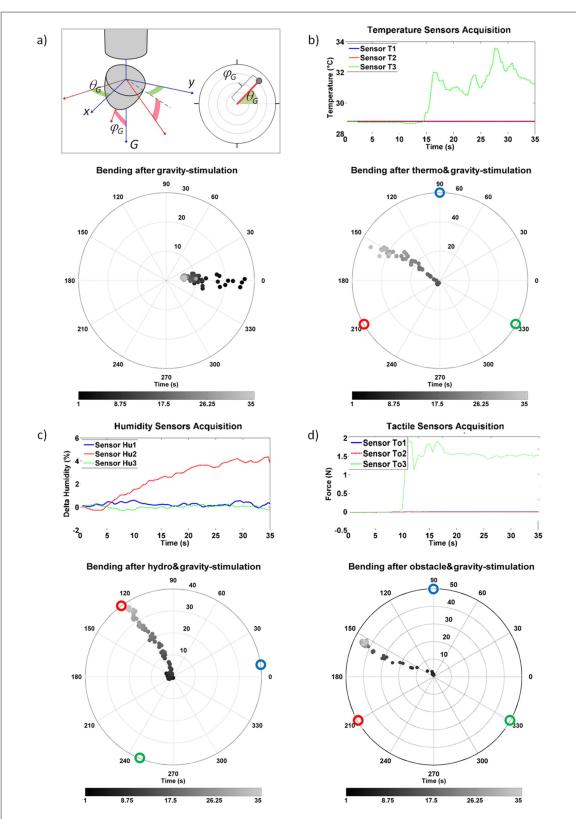
Figure 5. Dots in the polar plots represent the position of the apex with respect to its integral coordinate system. The inset shows the position of a general point in polar graph as a function of the experimental angles: in particular the polar plots express as radius the inclination angle with respect to the gravity (φ_G) and as polar angles the angle with respect to the x-axis (θ_G). Grey level of dots is a function of experimental time, as reported in the colour bar under each circular graph. If the apex is aligned with the gravity the graph would show a dot in the reference point (0, 0). (a) Polar plot of the accelerometer output for a root with an initial inclination of approximately 30°. (b) Polar plot of the accelerometer output for a root under thermo-stimulation of sensor T_3 (bottom) and relative sensor output plot during the experimentation period (top). (c) Polar plot of the accelerometer output for a root under hydro-stimulation of sensor Hu_2 (bottom) and relative sensor output plot during the experimentation period (top). (d) Polar plot of the accelerometer output for a root under obstacle-stimulation of touch sensing element To_3 (bottom) and relative sensing element output plot during the experimentation period (top). As reference, coloured circles report the position of the selected sensors with respect to the orientation of the polar graph.

Table 2. Bending angle variations with temperature, humidity and obstacle stimuli combined with gravity at different priority values.

	Bending angles obtained after stimulation combined with gravity		
K_G	Thermo	Hydro	Obstacle
0.3	44.39°	34.75°	30.58°
0.5	33.81°	15.66°	14.42°
0.7	18.94°	5.45°	5.96°

In each experiment the sensorized root apex (figure 4(b)) is originally aligned with the driving unit, but after the stimulation we could observe the deviation induced in the bending region characterised by SSBAs.

3.1. Gravitropism

To test the gravitropism, we placed the entire root at different inclinations and different directions with respect to its coordinate system. In each test, we obtained a bending of the apex towards the gravity vector.

From the graph reported in figure 5(a), it is possible to deduce the movement from the starting inclination, approximately 30°, toward the centre to align the apex with the gravity vector. The task is performed by the apex in a period less than 10 s. The attraction to gravity is expressed in DNA with the maximum priority and is the only attraction in $R_{(t)}$.

When decreasing the priority level of gravity in DNA, we obtained the same behaviour actuated with different speeds (lower priority, lower speed).

3.2. Thermotropism

We performed the thermotropism test on each embedded sensor obtaining analogous results: a bending away from the stimulus due to the high temperature imposed.

Figure 5(b) shows the results obtained during the stimulation for sensor T_3, which is placed at 330°. The priorities given to the tropisms are $K_G = 0.3$, $K_T = 0.7$. The figure shows the correlation between the bending obtained and the data acquired from the temperature sensors: without high variation among the three sensors acquisition, the tip does not move from its position, but when there is a variation (after approximately 15 s), the root starts to move in the direction along the circumference with the lower distance between the temperature acquired and the optimal value defined in DNA.

3.3. Hydrotropism

As for thermotropism, we performed the hydrotropism test on each sensor integrated in the apex. In the case of hydrotropism, we obtained a bending towards the highest concentration of water detected.

Figure 5(c) shows the results obtained by stimulating mostly the sensor Hu_2 and assigning $K_G = 0.3$ and $K_{Hu} = 0.7$: when there is an increase in water at 130°, the apex begins to adjust its bending in the direction of the resultant stimulus. Due to the low resistivity of the humidity sensors (approximately 5–600 Ω) and the conditioning circuit based on shunt resistors, with the relatively high resistance of 3.3 KΩ to avoid sensor overheating, the measure is digitally mediated using a moving average filter of 3.5 s width to minimise the noise effect. Moreover, to further decrease the heating of the sensors, the voltage to the reading circuit was applied only during the measurement (3 ms per second).

3.4. Thigmotropism

In the case of thigmotropism, we also stimulated the three lateral sensing elements, and we observed the negative response of the tropism implemented in the root as obstacle avoidance through bending in the opposite direction from the stimulus. In the example reported in figure 5(d), it is possible to observe the bending of the tip away from 330°, where the stimulated sensor was located (To_3), while the obstacle is present; figure 5(d) (top part) shows the sensor response to the obstacle. The priorities assigned in DNA for this experiment are $K_G = 0.3$, $K_{To} = 0.7$.

Assigning different priorities to the tropisms, we obtained different bending angles at the end of the experiments. The results are reported in table 2. When gravity has low priority (i.e. the attraction for gravity is reduced), a bending degree is higher than in the case of high priority, and the root follows the other stimuli. We would in fact need an extremely high stimulus against gravity to obtain a bigger bending angle. From the resulting behaviour, we can assert the importance of gravity in the balance of the system.

4. Conclusions

This paper presents the first robot prototype inspired by plants and, in particular, by the movements, sensing capabilities, and behaviours of their roots.

This robot, named Plantoid, integrates artificial roots able to respond to environmental conditions and stimuli, performing bending movements and obstacle avoidance response. Each robotic root integrates three SSBAs, which imitate the differential bending capability of plant roots through the differential elongation of the actuators, obtained by the direct assembly of helical springs on the shafts of DC gear-motors.

Each robotic root apex embeds a matrix of commercial gravity and temperature sensors and innovative sensors for touch and humidity, *ad hoc* customised for the specific robotic root application. The intrinsic flexibility of our tactile sensing arrays allowed us to shape them on the surface of the apex, while the high sensitivity of our humidity sensors

provides reliable measures without direct contact with soil, addressing challenges involving soil quality and compactness. The combination of the sensors and a root-inspired behaviour algorithm allowed the robotic roots to move and follow external stimuli in air. The modularity of the electronics and of the developed control allows a direct porting to the next generation of roots, where growing and bending capabilities will be integrated as unified solution suitable for penetration tasks. We performed several tests to show the robot capabilities in imitating the tropic behaviour of plant roots (i.e., gravitropism, hydrotropism, thigmotropism, and thermotropism) with different priority settings of the stimulus.

The proposed robot integrates different plant-inspired technologies and strategies that are innovative in the robotics field. The development of new sensors based on soft materials, as well as distributed control and robotic architectures, open new scenarios in the soft robotics context. We validated the root-inspired behaviour algorithm through the embedded sensing capabilities using the robotic system as a test platform. In the long term perspective, several applications can be envisaged for our plant-inspired technologies, including soil monitoring and exploration for contamination or mineral deposits—whether on earth or other planets, as well as in rescue, where the use of an autonomous non-invasive robot can be beneficial, and in agriculture.

Acknowledgments

References

[1] Hodge A 2004 The plastic plant: root responses to heterogeneous supplies of nutrients *New Phytol.* **162** 9–24

[2] Kiss J Z 2007 Where's the water? Hydrotropism in plants *Proc. Natl Acad. Sci.* **104** 4247–8

[3] Verbelen J P, De Cnodder T, Le J, Vissenberg K and Baluška F 2006 The root apex of arabidopsis thaliana consists of four distinct zones of growth activities *Plant Signaling Behavior* **1** 296–304

[4] Sadeghi A, Tonazzini A, Popova L and Mazzolai B 2014 A novel growing device inspired by plant root soil penetration behaviors *PLoS One* **9** e90139

[5] Mazzolai B, Mondini A, Corradi P, Laschi C, Mattoli V and Dario P 2011 A miniaturized mechatronic system inspired by plant roots *IEEE Trans. Mechatron.* **16** 201–12

[6] Sinibaldi E, Argiolas A, Puleo G L and Mazzolai B 2014 Another lesson from plants: the forward osmosis-based actuator *PLoS One* **9** e102461

[7] Taccola S, Greco F, Sinibaldi E, Mondini A, Mazzolai B and Mattoli V 2015 Toward a new generation of electrically controllable hygromorphic soft actuators *Adv. Mater.* **27** 1668–75

[8] Lucarotti C, Totaro M, Sadeghi A, Mazzolai B and Beccai L 2015 Revealing bending and force in a soft body through a plant root inspired approach *Sci. Rep.* **5** 8788

[9] Walker I D 2013 Continuous backbone continuum robot manipulators *ISRN Robot.* **2013** 726506

[10] Walker I D, Carreras C, McDonnell R and Grimes G 2006 Extension versus bending for continuum robots *Int. J. Adv. Robot. Syst.* **3** 171–8

[11] McMahan W *et al* 2006 Field trials and testing of the OctArm continuum manipulator *IEEE Int. Conf. on Robotics and Automation (ICRA) (Orlando, FL, USA)* pp 2336–41

[12] Suzumori K, Shoichi I and Hirohisa T 1991 Development of flexible microactuator and its applications to robotic mechanisms *IEEE Int. Conf. on Robotics and Automation (ICRA) (Sacramento, CA, USA)* pp 1622–7

[13] Renda F, Cianchetti M, Giorelli M, Arienti A and Laschi C 2012 A 3D steady-state model of a tendon-driven continuum soft manipulator inspired by the octopus arm *Bioinsp. Biomim.* **7** 025006

[14] Simaan N, Taylor R and Flint P 2004 A dexterous system for laryngeal surgery *IEEE Int. Conf. on Robotics and Automation (ICRA) (New Orleans, LA, USA)* pp 351–7

[15] Ataollahi A, Karim R, Fallah A S, Rhode K, Razavi R, Seneviratne L D, Schaeffter T and Althoefer K 2016 3-DOF MR-compatible multi-segment cardiac catheter steering mechanism *IEEE Trans. Biomed. Eng.* **63** 2425–35

[16] Mircea I, Bizdoaca N and Pana D 2003 Dynamic control for a tentacle manipulator with SMA actuators *IEEE Int. Conf. on Robotics and Automation (ICRA) (Taipei)* pp 2079–84

[17] Mazzolai B, Margheri L, Cianchetti M, Dario P and Laschi C 2012 Soft-robotic arm inspired by the octopus: II From artificial requirements to innovative technological solutions *Bioinsp. Biomim.* **7** 025005

[18] Tondu B and Pierre L 2000 Modeling and control of McKibben artificial muscle robot actuators *Control Syst.* **20** 15–38

[19] McMahan W, Jones B A and Walker I D 2005 Design and implementation of a multi-section continuum robot: air-octor *IEEE/RSJ Int. Conf. on Intelligent Robots and Systems (IROS) (Edmonton, Alberta, Canada)* pp 2578–85

[20] Maghooa F, Stilli A, Noh Y, Althoefer K and Wurdemann H A 2015 Tendon and pressure actuation for a bio-inspired manipulator based on an antagonistic principle *IEEE Int. Conf. on Robotics and Automation (ICRA) (Seattle, WA, USA)* pp 2556–61

[21] Stilli A, Wurdemann H A and Althoefer K 2014 Shrinkable stiffness-controllable soft manipulator based on a bio-inspired antagonistic actuation principle *IEEE/RSJ Int. Conf. on Intelligent Robots and Systems (IROS) (Chicago, IL, USA)* pp 2476–81

[22] Baluška F, Mancuso S, Volkmann D and Barlow P 2004 Root apices as plant command centres: the unique 'brain-like' status of the root apex transition zone *Biologia (Bratislava)* **59** 7–19

[23] Ciszak M, Comparini D, Mazzolai B, Baluška F, Arecchi F T, Vicsek T and Mancuso S 2012 Swarming behavior in plant roots *PLoS One* **7** e29759

[24] Timoshenko S P and Gere J M 1961 *Theory of Elastic Stability* (New York: McGraw-Hill)

[25] Webster R J III and Jones B A 2010 Design and kinematic modeling of constant curvature continuum robots: a review *Int. J. Robot. Res.* **1** 1–22

[26] Viry L, Levi A, Totaro M, Mondini A, Mattoli V, Mazzolai B and Beccai L 2014 Flexible three-axial force sensor for soft and highly sensitive artificial touch *Adv. Mater.* **26** 2659–64

[27] Lucarotti C, Totaro M, Viry L, Beccai L and Mazzolai B 2014 Soil mechanical impedance discrimination by a soft tactile sensor for a bioinspired robotic root *Biomimetic and Biohybrid Systems (Lecture Notes in Artificial Intelligence (LNAI))* ed A Duff *et al* vol 8608 (Berlin: Springer) pp 408–10

[28] Kawano K, Pacios R, Poplavsky D, Nelson J, Bradley D D C and Durrant J R 2006 Degradation of organic solar cells due to air exposure *Sol. Energy Mater. Sol. Cells* **90** 3520–30

[29] Huang J, Miller P, Wilson J, De Mello A J, De Mello J C and Bradley D C 2005 Investigation of the effects of doping and post-deposition treatments on the conductivity, morphology, and work function of poly(3,4-ethylenedioxythiophene)/poly (styrene sulfonate) films *Adv. Funct. Mater.* **15** 290–6

[30] Liu J, Agarwal M, Varahramyan K, Berney E S IV and Hodo W D 2008 Polymer-based microsensor for soil moisture measurement *Sensors Actuators* B **129** 599–604

[31] Guo Z, Shin K, Karki A B, Young D P, Kaner R B and Hahn H T 2009 Fabrication and characterization of iron oxide nanoparticles filled polypyrrole nanocomposites *J. Nanopart. Res.* **11** 1441–52

[32] Greco F, Zucca A, Taccola S, Menciassi A, Fujie T, Haniuda H, Takeoka S, Dario P and Mattoli V 2011 Ultra-thin conductive free-standing PEDOT/PSS nanofilms *Soft Matter* **7** 10642–50

[33] Greco F, Fujie T, Taccola S, Ricotti L, Menciassi A and Mattoli V 2012 Micro and nanowrinkled conductive polymer surfaces on shape-memory polymer substrates: tuning of surface microfeatures towards smart biointerfaces *MRS Proc.* **1411** mrsf11-1411-ee09-21

[34] Taccola S, Greco F, Zucca A, Innocenti C, Fernández C D J, Campo G, Sangregorio C, Mazzolai B and Mattoli V 2013 Characterization of free-standing PEDOT:PSS/iron oxide nanoparticle composite thin films and application as conformable humidity sensors *ACS Appl. Mater. Interfaces* **5** 6324–32